

# Finding defects in disorder: Strain-dependent structural fingerprint of plasticity in granular materials <sup>F</sup>

Cite as: Appl. Phys. Lett. **119**, 241904 (2021); <https://doi.org/10.1063/5.0068508>

Submitted: 25 August 2021 • Accepted: 23 November 2021 • Published Online: 17 December 2021

Siqi Xiao, <sup>ID</sup> Han Liu, Enigma Bao, et al.

## COLLECTIONS

<sup>F</sup> This paper was selected as Featured



View Online



Export Citation



CrossMark

## ARTICLES YOU MAY BE INTERESTED IN

### A perspective of twisted photonic structures

Applied Physics Letters **119**, 240501 (2021); <https://doi.org/10.1063/5.0070163>

### Self-sustaining MoS<sub>2</sub> nanomechanical oscillators and feedback cooling

Applied Physics Letters **119**, 243506 (2021); <https://doi.org/10.1063/5.0063079>

### Low-frequency noise characteristics of GaN vertical PIN diodes—Effects of design, current, and temperature

Applied Physics Letters **119**, 243505 (2021); <https://doi.org/10.1063/5.0075498>



Timing is everything.  
Now it's automatic.

A new synchronous source measure system for electrical measurements of materials and devices

**Lake Shore**  
CRYOTRONICS

[Learn more](#)

# Finding defects in disorder: Strain-dependent structural fingerprint of plasticity in granular materials

Cite as: Appl. Phys. Lett. **119**, 241904 (2021); doi: [10.1063/5.0068508](https://doi.org/10.1063/5.0068508)

Submitted: 25 August 2021 · Accepted: 23 November 2021 ·

Published Online: 17 December 2021






View Online



Export Citation



CrossMark

Siqi Xiao,<sup>1,2</sup> Han Liu,<sup>2</sup>  Enigma Bao,<sup>2</sup> Emily Li,<sup>2</sup> Caroline Yang,<sup>2</sup>  Yiqun Tang,<sup>1</sup> Jie Zhou,<sup>1,a)</sup> and Mathieu Bauchy<sup>2,a)</sup> 

## AFFILIATIONS

<sup>1</sup>Key Laboratory of Geotechnical and Underground Engineering of Ministry of Education, Tongji University, Shanghai 200092, China

<sup>2</sup>Physics of Amorphous and Inorganic Solids Laboratory (PARISlab), University of California, Los Angeles, California 90095, USA

<sup>a)</sup>Authors to whom correspondence should be addressed: [bauchy@ucla.edu](mailto:bauchy@ucla.edu) and [zoujer@hotmail.com](mailto:zoujer@hotmail.com)

## ABSTRACT

When subjected to loads, granular materials tend to yield and exhibit some localized particle reorganizations. Due to the complex disordered structure of granular materials, it is challenging to identify the key preexisting defects in the static, unloaded structure that eventually promotes dynamical particle rearrangements once a load is applied. Here, based on discrete element simulations of an archetypal frictional granular material model, we introduce a machine learning framework that pinpoints such structural defects with unprecedented accuracy. We show that the optimal structural fingerprint of plastic flow defects depends on strain, wherein the plastic flow is governed by short-range defects at low strain but become dominated by medium-range defects at high strain.

Published under an exclusive license by AIP Publishing. <https://doi.org/10.1063/5.0068508>

Under small deformations or loads, disordered materials, such as glasses, gels, or granular materials, exhibit an initial reversible elastic response.<sup>1–3</sup> Beyond a certain critical threshold, they tend to feature some heterogeneous, irreversible plastic particle reorganizations.<sup>4–6</sup> Although, in crystalline materials, such a plastic flow is controlled by lattice defects (e.g., dislocations),<sup>5,7</sup> identifying the linkages between structure and plastic reorganizations in non-crystalline systems is challenging—especially since structural defects are ill-defined in disordered structures.<sup>8–10</sup> In glasses, the “soft spots” (that is, the regions that present high propensity for plastic reorganization) can be identified based on the local energy, stress, or vibrational modes.<sup>11–13</sup> However, such approaches are not directly applicable to granular materials, wherein particles interact by contact.<sup>14,15</sup>

Cubuk *et al.* introduced a machine-learned structural quantity called “softness,” which is constructed so as to be correlated with particle rearrangements in disordered solids.<sup>9,16–20</sup> However, this method requires some level of intuition to define a “fingerprint” for particles, that is, a set of heuristic features that are expected to influence their propensity to reorganize.<sup>21</sup> Although graph neural networks offer a promising pathway to bypass the need for such handcrafted features,<sup>21–23</sup> such models are challenging to interpret.

In this Letter, we introduce a machine-learned descriptor of plasticity, wherein the fingerprint, rather than being handcrafted, is constructed based on a large array of intuitive structural features describing both the short-range and medium-range environment<sup>24</sup> of each particle. By taking the example of an archetypal frictional granular material model subjected to shear, we show that this approach predicts the particles’ dynamics based on the sole knowledge of their initial static, unloaded structure. Importantly, our approach reduces the need for intuition for the fingerprint and yields an unprecedented accuracy, without compromising interpretability.

To illustrate our approach, we consider the canonical example of a two-dimensional frictional granular material model that is subjected to a pure shear deformation [see the inset in Fig. 1(a)]. In addition of offering a simple, computationally efficient model, the two-dimensional system chosen herein allows us to decrease the number of degrees of freedom of the particles. The system comprises 10 000 spherical particles with a constant density of 2.5 g/cm<sup>3</sup> (representative of sand grains). To avoid any local crystallization, the simulated system exhibits some degree of polydispersity, wherein the diameter of particles presents a uniform distribution with an average diameter  $d = 1.35$  mm and a width  $\Delta d = 0.70$  mm.<sup>14</sup> The interaction between

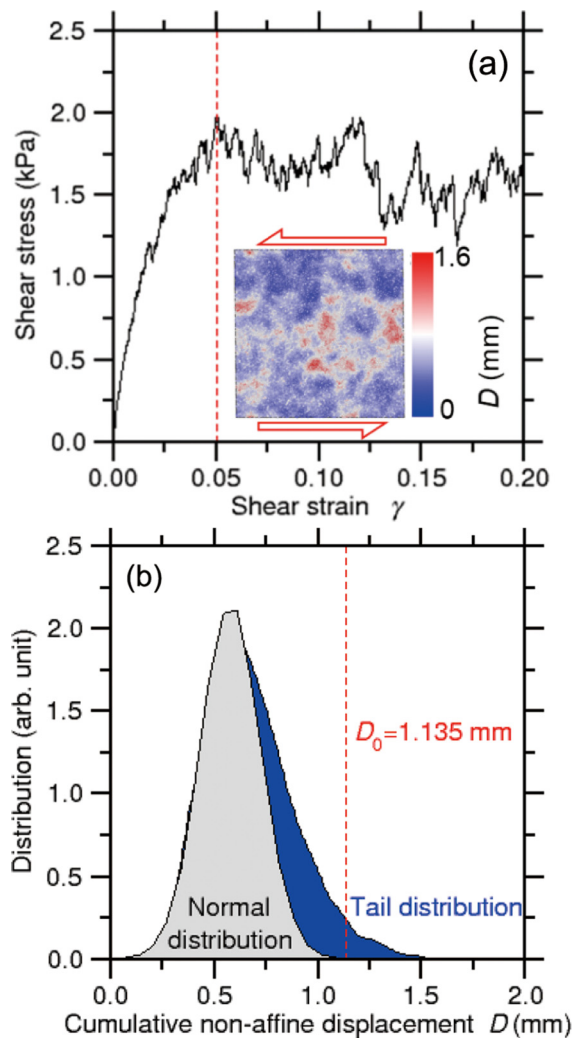


**FIG. 1.** (a) Computed stress–strain curve of the simulated granular material when subjected to a pure shear deformation. The inset shows the spatial distribution of the resulting cumulative non-affine displacement  $D$  for a shear strain  $\gamma = 5\%$ . The red dashed vertical line indicates the beginning of macroscopic yielding. (b) Distribution of the cumulative non-affine displacement  $D$  for a shear strain  $\gamma = 5\%$ . The data are fitted by a Gaussian distribution (grey area), and the right-tail deviation from the Gaussian distribution is highlighted in blue. The red dashed vertical line indicates the threshold ( $D_0$ ) that is used herein to discriminate immobile (low displacement) from mobile (high displacement) particles.

particles is described by a Hookean contact model, where the particles interact only by contact (when they overlap) via a repulsive linear spring model (spring-dashpot interaction) and static friction.<sup>25</sup> Details on the interaction model are provided in the [supplementary material](#). The initial configuration is prepared by randomly placing the particles in a square box while ensuring the absence of any overlap.<sup>26,27</sup> Prior to the shear deformation, the system is packed by imposing a high hydrostatic pressure (1 MPa) under periodic boundary conditions.<sup>28</sup> The system is then continuously relaxed by gradually decreasing the pressure down to zero. Once relaxed, the system is subjected to a pure shear deformation with a constant, fairly low

shear rate of  $5 \times 10^{-4} \text{ s}^{-1}$  following a standard athermal quasistatic protocol.<sup>12,29,30</sup> The time step is fixed at  $1 \times 10^{-5} \text{ s}$ . All simulations are conducted with LAMMPS.<sup>31</sup>

Figure 1(a) shows the computed shear stress as a function of the imposed shear strain. As expected, the system presents an initial fairly elastic regime at low strain, before displaying a plastic response at higher strain. Eventually, the granular system exhibits a plateau in shear stress once the shear strain exceeds 5%, which indicates complete yielding. We then further analyze the simulated trajectories to track the dynamics of the particles during the shear deformation. To isolate the local plastic particle reorganizations, we compute the cumulative non-affine displacement undergone by each particle during the deformation process.<sup>13</sup> Indeed, the non-affine square displacement  $D_{\min}^2$  metric has been extensively used to track plastic flow in disordered phases.<sup>6,17,29</sup> However, the conventional non-affine square displacement eventually becomes non-informative as the system starts to experience significant yielding since the structure becomes very different from its initial state. Here, to ensure that the deformed configurations are always compared to a meaningful reference, we adopt a cumulative non-affine displacement  $D$ , which is defined, for each particle, as the sum of the non-affine displacements experienced during small increments of strain:

$$D = \sum_{i=1}^n \sqrt{\Delta D_{i,\min}^2}, \quad (1)$$

where  $\Delta D_{i,\min}^2$  is the incremental non-affine square displacement after each small increment of strain  $i$  and  $n$  is the total number of strain increments. A local cutoff value of  $3d$  (where  $d$  is the average particle diameter) is used to compute the local affine displacement field. The incremental non-affine displacements are calculated every 1 s, that is, with a strain increment of  $5 \times 10^{-4}$ .

Figure 1(b) shows the distribution of the computed cumulative non-affine displacement  $D$  for a shear strain of 5%, that is, at the beginning of the macroscopic yielding regime [see Fig. 1(a)]. We observe that the distribution is centered around a low displacement value (i.e.,  $D = 0.56$  mm). This corresponds to the population of particles that do not exhibit any significant non-affine reorganization during the shear deformation. However, we note that the distribution also exhibits a long tail toward large displacement values [see Fig. 1(b)]. This suggests that a small portion of the particles feature some significant rearrangements, in agreement with previous studies.<sup>32,33</sup> In the following, we classify particles as “mobile” (soft) or “immobile” (hard) when their cumulative non-affine displacement  $D$  is larger or lower than the critical displacement threshold  $D_0 = 1.135$  mm, respectively (where  $D_0$  is equal to 81% of the average particle diameter  $d$ ). Based on this threshold, about 2% of the particles are classified as mobile. However, the following analysis does not significantly depend on the arbitrary choice of this threshold displacement (see the [supplementary material](#)).

We then adopt ML to derive a machine-learned structural fingerprint of plasticity, i.e., that is correlated with the propensity for particles to be mobile or immobile. The original softness approach uses as inputs some two- and three-body order parameters, which come with the advantage of offering a generic description of disordered networks, using a formalism that is transferable to various systems and scales.<sup>9</sup> In contrast, here, we use as input features a series of intuitive particle-

level structural properties, which are specifically selected so as to be the most informative for the system considered herein. Although this set of features is less transferable than those considered in the original softness approach, it has the advantage of offering a more condensed (i.e., lower dimensionality) and interpretable description of the structure of the present granular system (see below). These features are detailed in the [supplementary material](#) (see Fig. S2) and can be classified into different categories: (i) *connectivity* (e.g., number of contact points with neighbors), (ii) *radial environment* (e.g., average distance with neighbors), (iii) *angular environment* (e.g., average angle formed with neighbors), (iv) *packing* (e.g., Voronoi volume), and (v) *medium-range order* (wherein, for a central particle, the values of the previous features are recalculated for each of its first-coordination neighbors). Altogether, this results in a total of 76 features for each particle. We then conduct a feature selection analysis to identify the most influential structural properties to be used as inputs (see below). Here, we deliberately restrict the choice of the features to those that are simple, intuitive, easily interpretable and that can be solely computed from the static initial configuration (before any shearing is applied) although some features like local inversion symmetry have a strong influence on softness.<sup>34,35</sup> Overall, we envision that this “dictionary” of structural features could serve as a universal fingerprint to characterize the short- and medium-range order of particles in disordered networks.

Using the previous features as inputs, we train a classifier aiming to categorize particles as mobile or immobile. For each particle, the input feature vector is calculated based on the initial configuration of the system (before any load) and the output class (mobile or immobile) is determined from its cumulative non-affine displacement after a shear strain  $\gamma = 5\%$ , i.e., after 100 s of dynamics. All the features are standardized prior to any training. Consequently, the obtained weights are unitless and their magnitude can be directly compared to estimate the relative influence of each input feature. The dataset is then randomly split into training (80%) and test (20%) sets. In contrast with the original softness approach,<sup>9</sup> we adopt logistic regression,<sup>36</sup> which offers great model simplicity, accuracy, and interpretability.<sup>37</sup> Detail on hyperparameters optimization is provided in the [supplementary material](#). Finally, we use backward elimination to conduct a feature selection analysis,<sup>38</sup> wherein the number of features is gradually reduced so as to maximize the test set accuracy of the model (see Fig. S4). Eventually, 24 features are selected. Although some features indeed exhibit some level of correlation, the pair correlation coefficients remain fairly low (see Fig. S5). These trends are also stable upon independent training repetitions of the model. This suggests that the mapping that is learned by the classifier is not notably affected by the interdependency of the input features. For purposes of statistical averaging, the model is then trained and tested based on 200 random train/test splits.

The trained logistic regression classifier yields a hyperplane that discriminates mobile from immobile based on the initial structure of the granular system. We obtain an average accuracy of 72% and 71% and a weighted F1 score of 0.816 and 0.815 for the training and test sets, respectively. To illustrate the recall of the classifier, Fig. 2(a) shows the positions of the particles that are predicted to be mobile together with the ground-truth cumulative non-affine displacement field. We observe that the particles that are predicted to be mobile are indeed largely located within soft regions associated with large cumulative non-affine displacements. Importantly, our model offers an increase in

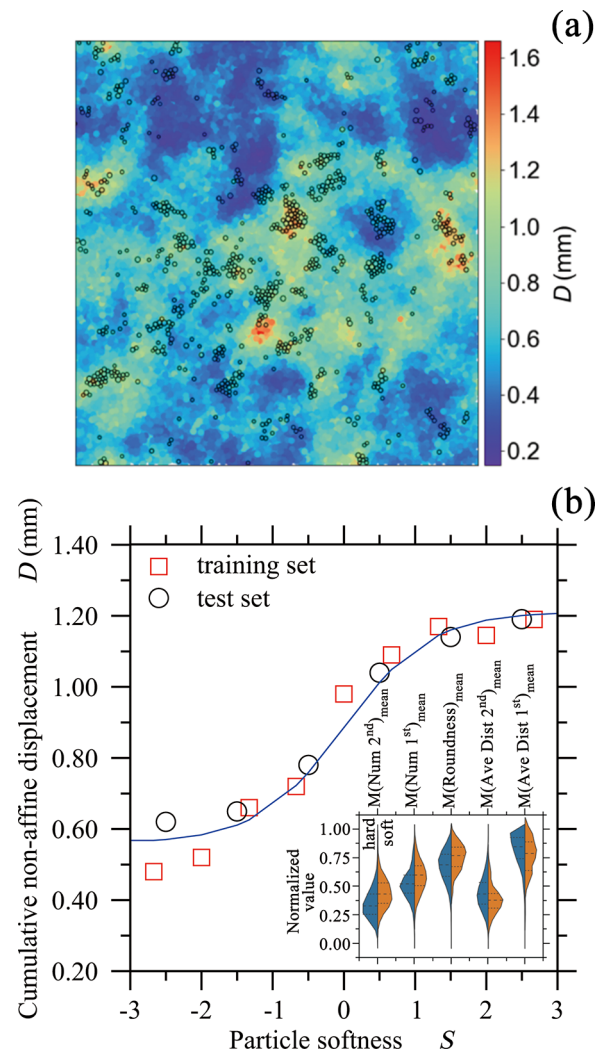


**FIG. 2.** (a) Spatial distribution of the cumulative non-affine displacement ( $D$ ) of the particles in the simulated granular material under a shear strain  $\gamma = 5\%$ . For comparison, the particles that are predicted to be “mobile” based on their local structure by the present machine learning classifier model are indicated in black. (b) Average non-affine displacement  $D$  of the particles in the training and test sets (at  $\gamma = 5\%$ ) as a function of their initial softness (calculated from their initial local structure). The solid line is to guide the eye.

accuracy as compared that offered by the original softness approach. Although this increase in accuracy is limited, it is significant since, in turn, our model uses fewer input features (24 vs 54 for the original softness approach). The lower dimensionality of the model is key to limit the “curse of dimensionality” and reduce the risk of overfitting when training the classifier (see the [supplementary material](#)). These results confirm that, in the case of the system simulated herein, the dynamics of the particles under load is largely encoded in its initial structure (before any load is applied). As shown in the inset (see the [supplementary material](#)) in Fig. 2(b), the structure-dynamics relationship is too complex to be described by a single intuitive structural metric. The fact that there does not exist a perfect mapping between



non-affine displacement and softness fields is a manifestation of the fact that our model does not exhibit a 100% classification accuracy.

The softness  $S$  of each particle is then defined as the orthogonal distance from the hyperplane of its position in the feature space. Mobile (soft) and immobile (hard) particles are associated with  $S > 0$  and  $S < 0$ , respectively. Figure 2(b) shows the average cumulative non-affine displacement  $D$  of the particles (averaged per bin of softness) as a function of their initial softness  $S$ . Interestingly, we find that, in addition to properly classifying the mobile and immobile particles, the distance from the decision boundary hyperplane (i.e., the softness  $S$ ) is itself highly correlated with the displacement of the particles—for both the training and test sets. That is, the propensity for the particles to exhibit reorganizations upon shear increases with softness and vice versa. In that regard, it is notable that, despite being subjected to a shear strain of 5% and total dynamics of 100 s, the system largely keeps the memory of the machine-learning softness metric (which is computed based on the initial structure of the system, before any load is applied).

Next, we focus on the interpretation of the classifier. The decision boundary hyperplane determined by logistic regression can be expressed in terms of the  $n$  features  $x_i$ ,

$$\sum_{i=1}^n \beta_i \cdot x_i + \beta_0 = 0, \quad (2)$$

where  $\beta_0$  is the intercept and  $\beta_i$  are the logistic regression parameters associated with each feature. Here, since all the features are standardized, the parameters  $\beta_i$  are directly indicative of the weight of each feature—wherein the axes associated with the most influential features (large  $|\beta_i|$ ) are the most orthogonal to the hyperplane. The signs of the parameters  $\beta_i$  also indicate whether the associated features have a positive or negative influence on the propensity for the particles to be mobile. Hence, the linear nature of the classifier adopted herein allows us to directly quantify the influence of each feature.

Figure 3(a) shows the absolute value of the weights of the 10 most influential features. Note that the features calculated within the medium-range order of the particles (see above) are denoted as  $M()$ . Overall, this interpretation analysis offers a series of insights, e.g., mobile particles tend to exhibit low contact numbers, larger distance with neighbors, and large local free space (see the [supplementary material](#)). Overall, we find that all the features have a notable influence on the classification—since non-influential features are already filtered out during the feature selection process. Note that none of these features would be a robust descriptor of particle reorganizations on its own. This illustrates the interest of the present machine learning approach—since the structure-dynamics relationship is too complex to be described by a single intuitive structural metric. Here, we find that the classifier is dominated by medium-range order structural features. Specifically, the average first- and second-shell coordination numbers of the neighbors of a central particle feature the largest influence. This can be understood from the fact that particles having an excess of neighbors tend to exhibit irregular, unstable local environments, wherein the neighbors form an irregular “zig zag” path rather than a well-defined circle (see Fig. S11 for an illustration of this feature). Such local instability promotes particle rearrangements under load. This indicates that, for this total strain (5%), the propensity for particles to rearrange is primarily encoded in their initial medium-

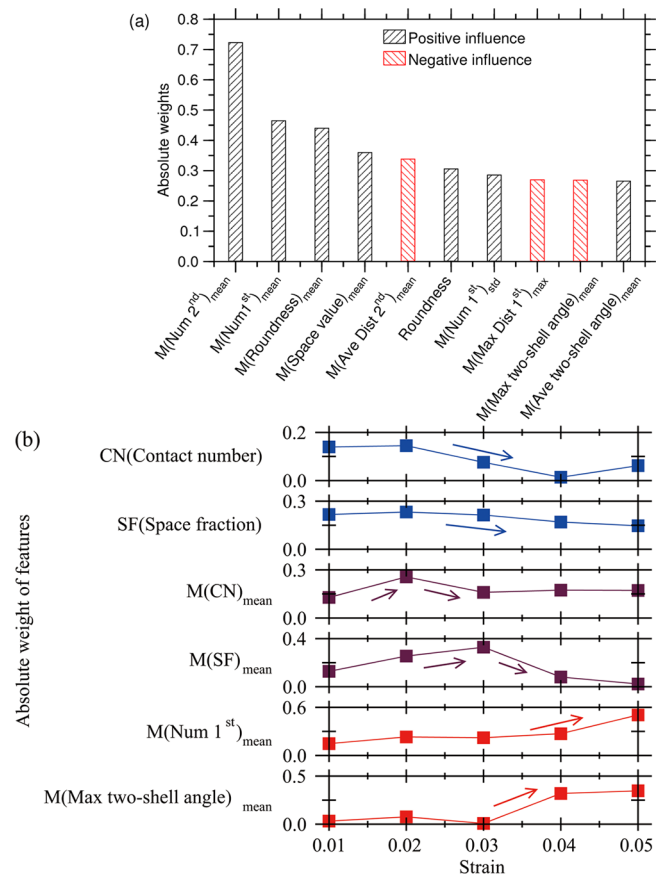


**FIG. 3.** (a) Ranking of the 10 structural features that are the most influential in the classifier (for a shear strain  $\gamma = 5\%$ ). The notation  $M()$  denotes that the features are calculated in the medium-range order of the particles (see the text and the supplemental material). Features highlighted in black and red are positively and negatively correlated with softness, respectively. (b) Variation of the influence of select features on the classifier as a function of the imposed shear strain. The notation  $M()$  denotes that the features are calculated in the medium-range order of the particles (see the text).

range order structure while, in turn, their initial short-range order structure has little influence, if any.

Finally, we explore how the influence of each structural feature depends on the applied shear strain. We compute the cumulative non-affine displacement of the particles at different strains, ranging from 1% to 5% with an increment of 1%. Five independent classifiers are trained to predict the mobile/immobile class of the particles for each strain while using the same initial structure for the input features. The hyperparameters of each classifier are independently optimized so as to maximize the test set accuracy. For consistency, the five classifiers are trained by using the same 24 structural features as inputs, which are reselected based on their overall influence for each of the five strains. All the classifiers exhibit a satisfactory average test set accuracy ( $> 65\%$ , see the [supplementary material](#)).

Figure 3(b) shows the evolution of the influence of the most informative features as a function of strain. Interestingly, we find that

the relative influence of the features is notably different at low and high strain. Note that a weight of 0.20 separates top-10 features (i.e., influential features) from most other features (i.e., weakly influential features), which tend to have a weight lower than 0.10. Specifically, we observe that the features describing the very short-range order of the particles (number of contact points and local free volume fraction) are largely influential at low strain (i.e., during the early dynamics of the particles) but become weakly influential at high strain. In contrast, the influence of medium-range order features (e.g., average coordination numbers of the neighbors) tend to gradually increase upon increasing strain. This indicates that, upon shearing, the dynamics of the particles gradually shifts from being short-range-order- to medium-range-order-dominated.

This can be understood as follows. At low strain, the low elastic energy provided to the system only enables the rearrangement of particles featuring short-range defects (e.g., coordination mismatch and large local free space)—since such localized rearrangements are associated with fairly low energy barriers. Such local rearrangements “reset” the short-range order structure of the particles, so that the particles that are mobile at low strain tend to lose the memory of their initial short-range order. As strain increases, such initial short-range defects get exhausted. In turn, at higher strain  $\gamma$ , the available elastic energy (which roughly scales with  $\gamma^2$ ) becomes large enough to induce collective reorganizations enabled by medium-range order soft spots, associated with larger energy barriers. Eventually, the available elastic energy resulting from the imposed strain ( $\gamma > 5\%$ ) becomes large enough to result in the complete yielding of the system.

We envision that the influential structural features identified herein and summarized in Fig. 3(a) could be compared with results obtained from x-ray tomography, which can be used to track the dynamics of grains in granular materials. Specifically, the fact that particle rearrangement is promoted by the existence of unstable local environments echoes the fact that highly distorted coplanar tetrahedra have been noted to enhance plasticity.<sup>39</sup> In addition, revealing the key structural features that are the most influential in governing the dynamics of the particles could offer useful insights to engineer novel materials with either enhanced plasticity (to increase their toughness) or, in contrast, improved stability.

Overall, these results highlight the fact that, in the case of the present two-dimensional archetypical granular material, the load-induced particle dynamics is largely encoded in its static initial structure, before any load is applied. However, the structure-dynamics relationship is complex and cannot be fully described by a single intuitive structural metric. In that regard, machine learning offers a powerful tool to “find needles in haystacks,” that is, to construct structural descriptors that exhibit maximum correlation with dynamics. Importantly, in contrast to “black-box” machine learning models presenting low interpretability, the present classifier offers a series of useful physical insights. Specifically, the present results reveal that, in the case of the present system, the particle dynamics gradually transitions from being dominated by the short-range to the medium-range order structure of the particles. Additional studies are needed to confirm that these results also apply to more complex three-dimensional granular materials or different loading conditions (e.g., different state of stress or deformation rates). We envision that the present machine learning framework (including the introduced dictionary of structural features and the interpretable classifier model) is generic to disordered systems and

could be applied to other load conditions (e.g., creep and vibrations) or material (e.g., glass and colloidal gels).

See the [supplementary material](#) for the details about hyperparameter selection for the machine learning method.

This work was supported by the National Science Foundation (under Grant Nos. DMREF-1922167 and DMR-1944510), the National Science Foundation of China (under Grant No. 41572285), and the China Scholarship Council (under Grant No. 201906260205).

## AUTHOR DECLARATIONS

### Conflict of Interest

The authors have no conflicts to disclose.

## DATA AVAILABILITY

The data that support the findings of this study are available from the corresponding authors upon reasonable request.

## REFERENCES

- <sup>1</sup>M. Singh, M. Ozawa, and L. Berthier, *Phys. Rev. Mater.* **4**, 025603 (2020).
- <sup>2</sup>M. Bauchy, M. Wang, Y. Yu, B. Wang, N. A. Krishnan, E. Masoero, F.-J. Ulm, and R. Pellenq, *Phys. Rev. Lett.* **119**, 035502 (2017).
- <sup>3</sup>K. Karimi and J.-L. Barrat, *Sci. Rep.* **8**, 4021 (2018).
- <sup>4</sup>M. Ozawa, L. Berthier, G. Biroli, and G. Tarjus, *Phys. Rev. Res.* **2**, 023203 (2020).
- <sup>5</sup>J. Rottler, S. S. Schoenholz, and A. J. Liu, *Phys. Rev. E* **89**, 042304 (2014).
- <sup>6</sup>M. L. Falk and J. S. Langer, *Phys. Rev. E* **57**, 7192 (1998).
- <sup>7</sup>A. Seeger, *London, Edinburgh, Dublin Philos. Mag. J. Sci.* **46**, 1194 (1955).
- <sup>8</sup>L. Berthier, *Physics* **4**, 42 (2011).
- <sup>9</sup>E. Cubuk, S. Schoenholz, J. Rieser, B. Malone, J. Rottler, D. Durian, E. Kaxiras, and A. Liu, *Phys. Rev. Lett.* **114**, 108001 (2015).
- <sup>10</sup>L. Tian, Y. Fan, L. Li, and N. Mousseau, *Scr. Mater.* **186**, 185 (2020).
- <sup>11</sup>S. Patinet, D. Vandembroucq, and M. L. Falk, *Phys. Rev. Lett.* **117**, 045501 (2016).
- <sup>12</sup>J. Ding, S. Patinet, M. L. Falk, Y. Cheng, and E. Ma, *Proc. Natl. Acad. Sci. U. S. A.* **111**, 14052 (2014).
- <sup>13</sup>L. Tang, H. Liu, G. Ma, T. Du, N. Mousseau, W. Zhou, and M. Bauchy, “The energy landscape governs ductility in disordered materials,” *Mater. Horizons* **8**(4), 1242–1252 (2021), <https://pubs.rsc.org/en/content/articlelanding/2021/mh/d0mh00980f/unauth>.
- <sup>14</sup>G. Lois, A. Lemaître, and J. M. Carlson, *Phys. Rev. E* **72**, 051303 (2005).
- <sup>15</sup>R. Sain, T. Mukerji, and G. Mavko, *Geophysics* **81**, D561 (2016).
- <sup>16</sup>E. D. Cubuk, S. S. Schoenholz, E. Kaxiras, and A. J. Liu, *J. Phys. Chem. B* **120**, 6139 (2016).
- <sup>17</sup>E. D. Cubuk, R. J. S. Ivancic, S. S. Schoenholz, D. J. Strickland, A. Basu, Z. S. Davidson, J. Fontaine, J. L. Hor, Y.-R. Huang, Y. Jiang, N. C. Keim, K. D. Koshigan, J. A. Lefever, T. Liu, X.-G. Ma, D. J. Magagnosc, E. Morrow, C. P. Ortiz, J. M. Rieser, A. Shavit, T. Still, Y. Xu, Y. Zhang, K. N. Nordstrom, P. E. Arratia, R. W. Carpick, D. J. Durian, Z. Fakhraai, D. J. Jerolmack, D. Lee, J. Li, R. Riggleman, K. T. Turner, A. G. Yodh, D. S. Gianola, and A. J. Liu, *Science* **358**, 1033 (2017).
- <sup>18</sup>S. S. Schoenholz, E. D. Cubuk, D. M. Sussman, E. Kaxiras, and A. J. Liu, *Nat. Phys.* **12**, 469 (2016).
- <sup>19</sup>D. M. Sussman, S. S. Schoenholz, E. D. Cubuk, and A. J. Liu, *Proc. Natl. Acad. Sci. U. S. A.* **114**, 10601 (2017).
- <sup>20</sup>X. Ma, Z. S. Davidson, T. Still, R. J. Ivancic, S. Schoenholz, A. Liu, and A. Yodh, *Phys. Rev. Lett.* **122**, 028001 (2019).
- <sup>21</sup>V. Bapst, T. Keck, A. Grabska-Barwinska, C. Donner, E. D. Cubuk, S. S. Schoenholz, A. Obika, A. W. R. Nelson, T. Back, D. Hassabis, and P. Kohli, *Nat. Phys.* **16**, 448 (2020).

- <sup>22</sup>P. W. Battaglia, J. B. Hamrick, V. Bapst, A. Sanchez-Gonzalez, V. Zambaldi, M. Malinowski, A. Tacchetti, D. Raposo, A. Santoro, R. Faulkner, C. Gulcehre, F. Song, A. Ballard, J. Gilmer, G. Dahl, A. Vaswani, K. Allen, C. Nash, V. Langston, C. Dyer, N. Heess, D. Wierstra, P. Kohli, M. Botvinick, O. Vinyals, Y. Li, and R. Pascanu, [arXiv:1806.01261](#) [cs, stat] (2018), arXiv: 1806.01261.
- <sup>23</sup>A. Santoro, D. Raposo, D. G. T. Barrett, M. Malinowski, R. Pascanu, P. Battaglia, and T. Lillicrap, [arXiv:1706.01427](#) [cs] (2017), arXiv: 1706.01427.
- <sup>24</sup>Q. Wang and A. Jain, [Nat. Commun.](#) **10**, 5537 (2019).
- <sup>25</sup>P. A. Cundall and O. D. L. Strack, [Géotechnique](#) **29**, 47 (1979).
- <sup>26</sup>L. E. Silbert, D. Ertas, G. S. Grest, T. C. Halsey, and D. Levine, [Phys. Rev. E](#) **65**, 051307 (2002).
- <sup>27</sup>L. E. Silbert, D. Ertas, G. S. Grest, T. C. Halsey, and D. Levine, [Phys. Rev. E](#) **65**, 031304 (2002).
- <sup>28</sup>H. A. Makse, N. Gland, D. L. Johnson, and L. Schwartz, [Phys. Rev. E](#) **70**, 061302 (2004).
- <sup>29</sup>C. E. Maloney and A. Lemaître, [Phys. Rev. E](#) **74**, 016118 (2006).
- <sup>30</sup>B. Xu, M. L. Falk, J. Li, and L. Kong, [Phys. Rev. Lett.](#) **120**, 125503 (2018).
- <sup>31</sup>S. Plimpton, [J. Comput. Phys.](#) **117**, 1 (1995).
- <sup>32</sup>S. T. Bramwell, [Nat. Phys.](#) **5**, 444 (2009).
- <sup>33</sup>B. Kou, Y. Cao, J. Li, C. Xia, Z. Li, H. Dong, A. Zhang, J. Zhang, W. Kob, and Y. Wang, [Nature](#) **551**, 360 (2017).
- <sup>34</sup>A. Lemaître and C. Maloney, [J. Stat. Phys.](#) **123**, 415 (2006).
- <sup>35</sup>R. Milkus and A. Zaccane, [Phys. Rev. B](#) **93**, 094204 (2016).
- <sup>36</sup>C. Bishop, *Pattern Recognition and Machine Learning* (Springer, 2006).
- <sup>37</sup>H. Liu, S. Xiao, L. Tang, E. Bao, E. Li, C. Yang, Z. Zhao, G. Sant, M. M. Smedskjaer, L. Guo, and M. Bauchy, [Acta Mater.](#) **210**, 116817 (2021).
- <sup>38</sup>V. Kotu and B. Deshpande, in *Data Science (Second Edition)*, edited by V. Kotu and B. Deshpande, 2nd ed. (Morgan Kaufmann, 2019), pp. 467–490.
- <sup>39</sup>Y. Cao, J. Li, B. Kou, C. Xia, Z. Li, R. Chen, H. Xie, T. Xiao, W. Kob, L. Hong, J. Zhang, and Y. Wang, [Nat. Commun.](#) **9**, 2911 (2018).